*Supported by a Doctoral Award from Eastman Kodak Company.

[1]I. Giaever, Phys. Rev. Letters 20, 1286 (1968).
[2]I. Giaever and H. R. Zeller, J. Vac. Sci. Technol. 6, 502 (1969).
[3]I. Giaever and H. R. Zeller, Phys. Rev. Letters 21, 1385 (1968).
[4]M. L. A. MacVicar, S. M. Freake, and C. J. Adkins, J. Vac. Sci. Technol. 6, 717 (1969).
[5]R. C. Jaklevic and J. Lambe, Phys. Rev. Letters 17, 1139 (1966).
[6]J. F. Parrish, C. H. Perry, O. Brafman, I. F. Chang, and S. S. Mitra, in *II-VI Semiconducting Compounds*, edited by D. G. Thomas (Benjamin, New York, 1967), p. 1164; M. Balkanski, *ibid.*, p. 1007.
[7]J. L. Miles and P. H. Smith, J. Electrochem. Soc. 110, 1240 (1963).
[8]First- and second-derivative measurements were made using standard modulation techniques. Our circuitry was patterned after a design by A. Longacre, Jr. [Rev. Sci. Instr. 41, 448 (1970)].
[9]K. L. Chopra, *Thin Film Phenomena* (McGraw-Hill, New York, 1969), Chap. IV.
[10]M. Balkanski, R. Beserman, and J. M. Besson, Solid State Commun. 4, 201 (1966).

PHYSICAL REVIEW B VOLUME 3, NUMBER 6 15 MARCH 1971

Second-Order Raman Spectrum of MgO†

N. B. Manson,* W. Von der Ohe, and S. L. Chodos
Department of Physics, University of California, Los Angeles, California 90024
(Received 17 August 1970)

The second-order Raman spectrum of MgO at room temperature is reported for different polarizations and crystal orientations. The parts of the scattering polarizability transforming as A_{1g}, E_g, and T_{2g} are separated and compared with features in the two-phonon dispersion curves at the critical points Γ, X, L, and W.

INTRODUCTION

The lattice dynamics of MgO has been the subject of extensive experimental and theoretical investigations as can be seen from the numerous publications on the subject. These have included studies of neutron scattering,[1,2] infrared absorption,[3,4] and vibronic transitions of impurity ions.[5–8] However, there is a lack of reliable Raman data – those reported previously being in error[9] or incomplete.[10]

MgO has the rocksalt structure and hence shows no first-order Raman effect. The second-order spectrum has been clearly identified, and is reported here for different polarizations and crystal orientations. The strong features are considered to arise from points of high density of states near critical points in the Brillouin zone and, therefore, comparison is made to the two-phonon dispersion curves which have been constructed with the help of neutron data.[1,2]

EXPERIMENTAL

The exciting source was a Spectra Physics model 141 argon ion laser, which gave a multimode power of 300 mW in the 4880-Å line. The beam was focused on the crystal with a 3-cm-focal-length lens. An $f/1.5$ cone of light scattered at right angles was collected and dispersed by a Spex 1401 double monochromator. It was detected by a cooled ITT FW 130 photomultiplier using photoncounting techniques. The incident beam passed through a narrow bandpass interference filter in order to keep the nonlasing A^+ lines from distorting the spectra, and then through a double Fresnel rhomb. With the latter device the direction of polarization of the incoming beam could be rotated by 90°. The scattered beam was analyzed by a Polaroid sheet placed in front of the entrance slit. The final scans were recorded at a speed of 3 Å/min with a 5-sec time constant and a spectral slitwidth of 8 cm^{-1}.

Initially spectra were taken of six different MgO crystals and with three different laser lines. Two of the crystals were deliberately doped, the remaining four not. However, these crystals had all been grown in an electric arc furnace and are known to contain numerous kinds of impurities.[11] At least the coarse structure consisting of five broad peaks and one comparatively narrow one nearly at the center was observed in each case.

Two further phenomena were exhibited by every crystal and with every laser line: (i) The low-lying band peaked at 128 cm^{-1}, and (ii) a fluorescend background. Both can be seen in Fig. 1.

The intensity of the low-energy band varies little from sample to sample. It is assumed to be a difference band and is under further investigation. The fluorescence background represents the short-wavelength side of a broad smooth emission band, which reaches its peak at around 6000 Å. Its intensity varies from sample to sample and also within one specimen from point to point. This emission is thought to be caused by some imperfection which is present in all crystals but whose concentration is not constant. The final spectra, which

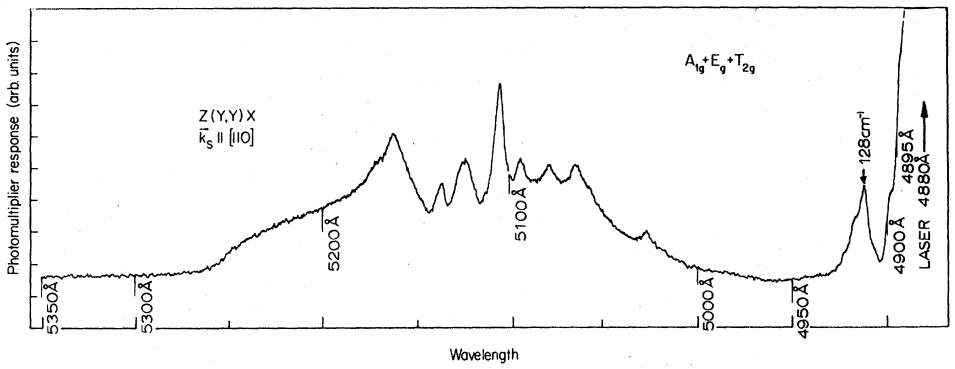

FIG. 1. Raman spectrum of MgO at room temperature; instrumental slit width 8 cm^{-1}. Note the relative strength of the fluorescence background to the Raman features. The low-frequency peak at 128 cm^{-1} is probably a difference band.

are reproduced in Figs. 1 and 2, were all taken from the same crystal. It was nominally pure with the convenient size of 27×8×4 mm and was cut perpendicular to the ⟨100⟩ directions. In addition, it had one face perpendicular to [110]. In this way, while the direction of the incident beam was kept constant at $\vec{k}_i \parallel [001]$, the scattered beam could be chosen either along $\vec{k}_s \parallel [100]$ or $\vec{k}_s \parallel [110]$.

MgO has O_h point-group symmetry and hence[12] the polarizability tensor has the irreducible representations A_{1g}, E_g, and T_{2g}. For the two orientations just described the Raman-intensity matrices[13,14] of modes which transform like these representations are compiled in Table I. The elements are directly proportional to the relative intensity of the Raman-active modes. They are obtained by (a) transforming the Raman tensors[12] to the laboratory frame of reference; (b) squaring the elements; and (c) in case of degenerate modes, adding them together. The laboratory system of coordinates is defined by the incident beam as Z axis and the scattered beam as X axis. An inspection of these matrices verifies immediately which type of "modes" or combination thereof is selected by the choices of crystal orientations and polarizations of Figs. 2(a)–2(d). For convenience they are listed in Table II.

Figures 2(b) and 2(c) display solely an E_g and a T_{2g} spectrum. The A_{1g} spectrum can never be obtained alone, and with the crystal orientations used some E_g contribution is simultaneously present. This can be subtracted out; the result of doing so is seen in Fig. 3. A fourth spectrum, Fig. 2(a), is included as a check of the consistency. It con-

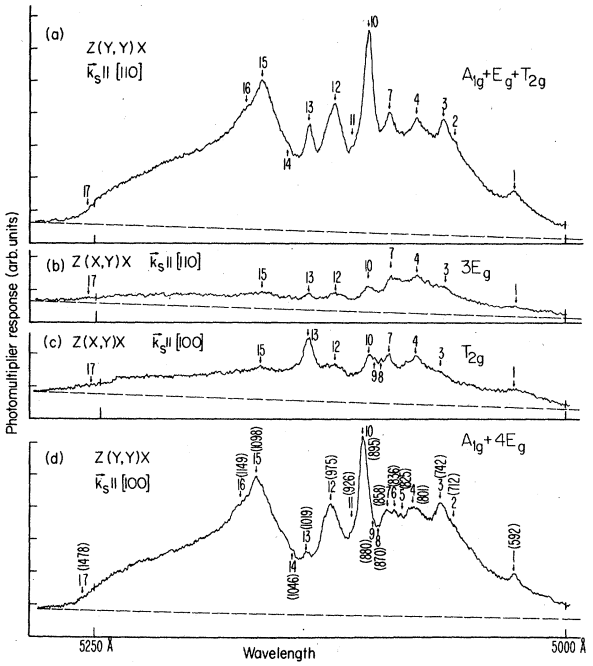

FIG. 2. Second-order Raman spectrum of MgO at room temperature for four different geometries using the 4880-Å argon ion laser line. Note that the zero has been displaced by a constant amount as can be seen by comparing Fig. 1 with (a) above. The peak positions and features are numbered with their positions in wave numbers given in trace (d); the weaker features indicated have been confirmed by comparison with several other traces.

TABLE I. Raman-intensity matrices.

Irreducible representation	$\vec{k}_s \parallel [100]$	$\vec{k}_s \parallel [110]$
A_{1g}	$a^2\begin{pmatrix}1&0&0\\0&1&0\\0&0&1\end{pmatrix}$	$a^2\begin{pmatrix}1&0&0\\0&1&0\\0&0&1\end{pmatrix}$
E_g	$b^2\begin{pmatrix}4&0&0\\0&4&0\\0&0&4\end{pmatrix}$	$b^2\begin{pmatrix}1&3&0\\3&1&0\\0&0&4\end{pmatrix}$
T_{2g}	$d^2\begin{pmatrix}0&1&1\\1&0&1\\1&1&0\end{pmatrix}$	$d^2\begin{pmatrix}1&0&1\\0&1&1\\1&1&0\end{pmatrix}$

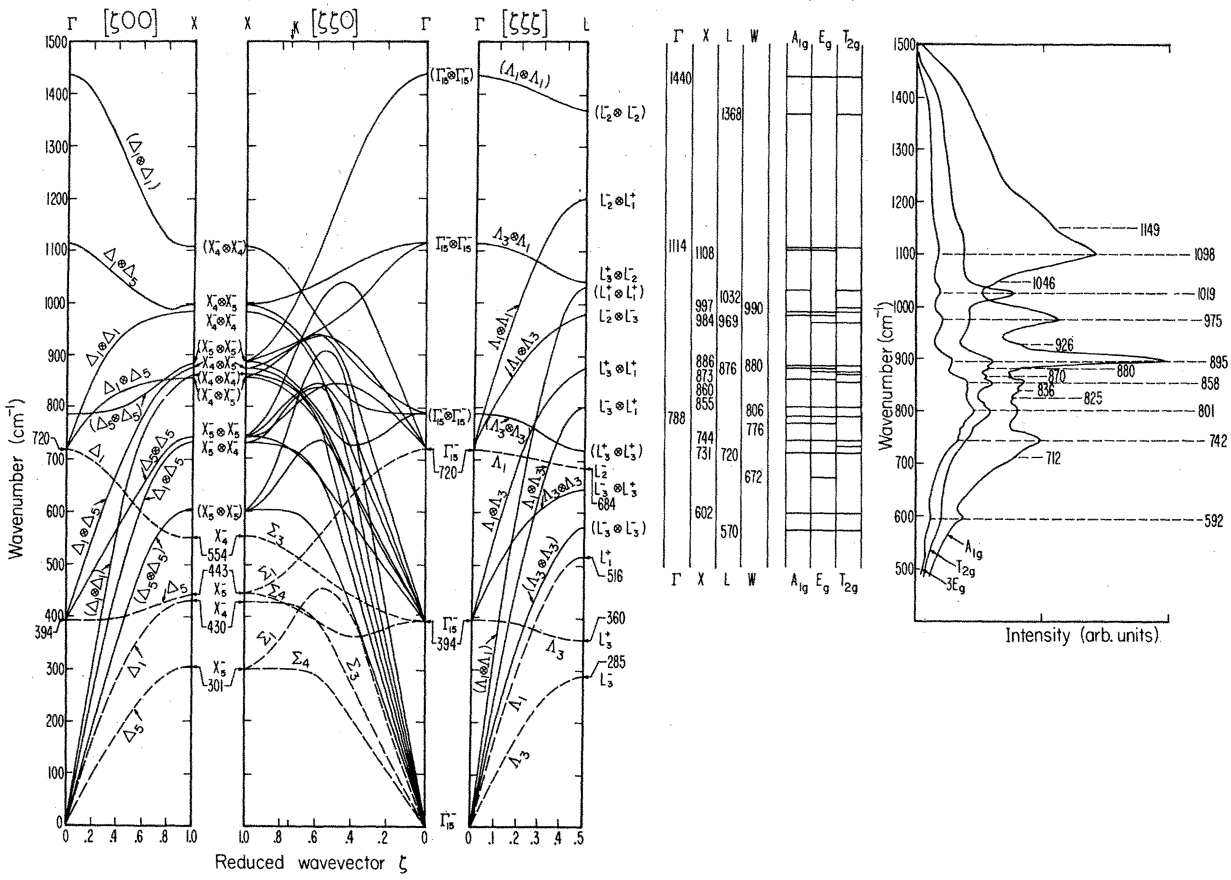

FIG. 3. Comparison of the two-phonon dispersion curves and second-order Raman spectrum. The dashed curves in the left-hand diagrams give the one-phonon dispersion curves (which had been constructed as described in the text). They are labeled according to their space-group symmetry. From these the two-phonon dispersion curves are constructed and labeled again as to their space-group symmetry – left as a direct product (or symmetric product for those with brackets) of the symmetries of the two one-phonon states. In the seven columns at the center, features from the critical points Γ, X, L, and W are indicated as to position and separately as to their transformation property. On the right-hand side are the experimentally determined distributions A_{1g}, E_g, and T_{2g} (where the fluorescence background is subtracted).

tains one unit each of A_{1g}, E_g, and T_{2g}.

All spectra were chosen such that the analyzer passed the Y component of the scattered radiation. This was done purposely in order to take advantage of the more sensitive direction of the monochromator. At the same time it avoided the insertion of a polarization scrambler or the application of a correction factor.

The crystal was always held at room temperature. Cooling to liquid-nitrogen temperature revealed no apparent change in the structure or in the relative strength of the main peaks. The whole spectrum was shifted slightly towards lower energies by an amount less than the spectral slitwidth.

DISCUSSION

In the two-phonon Raman effect, momentum considerations do not restrict the phonon wave vectors to $\vec{k} \approx 0$. Rather, the conservation of momentum becomes $\vec{k}_1 + \vec{k}_2 \approx N\vec{K}$, where $\vec{K}$ is a reciprocal-lattice vector and N may be zero. Thus $\vec{k}_1$ and $\vec{k}_2$ are only required to be members of the same star. The

TABLE II. Selected polarizations. The directions of polarization are expressed in the standard way (Ref. 15), with the letters indicating the direction of propagation of the incident and the scattered light being omitted, since they were kept constant at Z and X, respectively.

Orientation	Polarization	Modes	Figure
$\vec{k}_s \parallel [110]$	(Y, Y)	$A_{1g}+E_g+T_{2g}$	2(a)
	(X, Y)	$3E_g$	2(b)
$\vec{k}_s \parallel [100]$	(X, Y)	T_{2g}	2(c)
	(Y, Y)	$A_{1g}+4E_g$	2(d)

spectrum is expected to show structure which corresponds to the Van Hove singularities[16,17] in the combined density of states of pairs of vibrational modes which are associated with critical points in the $\omega(\vec{k}_1)+\omega(\vec{k}_2)$ dispersion curves (proper selection rules being taken into account). It is often assumed[18] that most of the structure in the observed spectra originates from the analytical critical points (X, L, W) near the Brillouin-zone boundary.

We have therefore constructed two-phonon dispersion curves (Fig. 3)[19] based on the neutron diffraction data of Peckham[1] and Sangster, Peckham, and Saunderson,[2] and also shell-model dispersion curves[11] where no neutron data exist.

TABLE III. Selection rules for Raman polarizability and infrared activity for MgO. The brackets around terms in the infrared-active column indicate they drop out when considering symmetric products.

Two-phonon combination	Raman polarization	Infrared active
$X_4^- \otimes X_4^-$	$A_{1g} + E_g$	
$X_4^- \otimes X_5^-$	T_{2g}	
$X_5^- \otimes X_5^-$	$A_{1g} + 2E_g + T_{2g}$	
$L_1^+ \otimes L_1^+$	$A_{1g} + T_{2g}$	
$L_1^+ \otimes L_3^+$	$E_g + T_{2g}$	
$L_1^+ \otimes L_2^+$		yes
$L_1^+ \quad L_3^+$		yes
$[L_3^+]^2$	$A_{1g} + E_g + 2T_{2g}$	
$L_3^+ \otimes L_2^-$, $L_3^+ \otimes L_3^-$		yes
$L_2^- \otimes L_2^-$	$A_{1g} + T_{2g}$	
$L_2^- \otimes L_3^-$	$E_g + T_{2g}$	
$[L_3^-]^2$	$A_{1g} + E_g + 2T_{2g}$	
$W_1 \otimes W_1$, $W_2' \otimes W_2'$	$A_{1g} + E_g$	
$W_1 \otimes W_2'$	E_g	yes
$W_1 \otimes W_3$, $W_2' \otimes W_3$	T_{2g}	yes
$W_3 \otimes W_3$	$A_{1g} + 2E_g + T_{2g}$	[yes]
$\Delta_1 \otimes \Delta_1$	$A_{1g} + E_g$	yes
$\Delta_1 \otimes \Delta_5$	T_{2g}	yes
$\Delta_5 \otimes \Delta_5$	$A_{1g} + E_g + T_{2g}$	[yes]
$\Sigma_1 \otimes \Sigma_1$, $\Sigma_3 \otimes \Sigma_3$, $\Sigma_4 \otimes \Sigma_4$	$A_{1g} + E_g + T_{2g}$	[yes]
$\Sigma_1 \otimes \Sigma_3$	T_{2g}	yes
$\Sigma_3 \otimes \Sigma_4$	T_{2g}	
$\Sigma_1 \otimes \Sigma_4$	E_g	yes
$\Lambda_1 \otimes \Lambda_1$	$A_{1g} + T_{2g}$	[yes]
$\Lambda_1 \otimes \Lambda_3$	$E_g + T_{2g}$	yes
$\Lambda_3 \otimes \Lambda_3$	$A_{1g} + E_g + 2T_{2g}$	[yes]

The representation formed by the pairs of phonons taking part in the second-order scattering process can be reduced to a sum of irreducible representations.[20] If this sum contains terms with the same symmetry as the polarizability tensor, the two-phonon state is Raman active. As noted above, the polarizability tensor for O_h symmetry transforms as $A_{1g}+E_g+T_{2g}$. The Raman-polarization selection rules for the two-phonon species at X, L, W, Δ, Σ, and Λ are given in Table III. For the particular points Γ, X, L, and W, these are repeated in Fig. 3 in a more convenient form. This information coupled with the experimentally determined polarization characteristics of each second-order peak (Fig. 3) should shed some light on which critical points in the Brillouin zone contribute to the second-order scattering. It should be noted that besides the analytic critical points at Γ, X, L, and W, there are undoubtedly contributions to the scattering coming from other high-density-of-states points along the zone boundary and within the zone. The extent to which these points contribute to the observed spectra is unknown.

It is clear, however, after a brief inspection of Fig. 3 that the dispersion curves compare favorably with experiment. Both the start and the end of the spectrum agree well with that expected. There is a gradual increase with an initial peak at 592 cm^{-1} corresponding with the lowest flat regions in the phonon dispersion curves at L(602 cm^{-1}) and X(570 cm^{-1}), and at the high-frequency end of the spectrum a cutoff with the anticipated shape and position around 1440 cm^{-1}. The first principal peak, predominantly A_{1g}, at 742 cm^{-1} agrees with a two-phonon dispersion branch which intersects the zone boundary at X with an energy of 744 cm^{-1}. The shoulder at 712 cm^{-1} could come from the overtone of the transverse optic branch at L(720 cm^{-1}). Both of these features are predicted to have scattering polarizabilities containing each of the three irreducible representations A_{1g}, E_g, and T_{2g}. There is evidence of seeing the same structure in all three polarizations, but the features are not nearly so predominant in E_g or T_{2g}. The next significant peak (No. 4, Fig. 2) at 801 cm^{-1} seen in all polarizations agrees with two features in the dispersion curves at Γ(788 cm^{-1}) and W(806 cm^{-1}) which are allowed by symmetry for all three polarizations. Perhaps the latter of these is preferred as it arises from the point W at the zone boundary where the density of phonon states is expected to be larger than at the zone center Γ. Between 825 and 895 cm^{-1} there are six peaks including the predominant feature of the spectrum at 895 cm^{-1}. In the phonon

dispersion curves there are also six features in this region, but they are much closer together, lying between 855 and 886 cm^{-1}. Only three are predicted to be visible in A_{1g}, whereas all six are seen in the A_{1g} distribution. Hence, some of the structure must arise from other points in the Brillouin zone. The strong sharp peak of A_{1g} character, however, would appear to arise from the overtone of the longitudinal optic branch which is exceptionally flat between X and W, varying from 886 to 880 cm^{-1}. For the other two symmetries the correspondence of the number of peaks is better; for T_{2g} four are expected and four are actually seen, and for E_g four are predicted of which at least two are clearly seen. Proceeding to 975 cm^{-1} (peak No. 12), there is another strong peak in the A_{1g} polarization. It is presumably associated with a flat region in the dispersion either at X(984 cm^{-1}) or at W(990 cm^{-1}), but it is difficult to decide between the two alternatives. The strong T_{2g} peak (No. 13), at 1019 cm^{-1}, which also appears in the E_g spectrum but not in A_{1g}, presents a slight mystery. Its position does not agree very closely with any predicted feature and leaves as a possible choice a branch at 1032 or at 997 cm^{-1}. However, both of these points are forbidden in E_g and hence attributing the peak to either must be considered doubtful. Lastly, there is the strong A_{1g} band peaked at 1098 cm^{-1} which stretches out on the high-energy side with a cutoff, as mentioned earlier, around 1440 cm^{-1}. This peak position makes excellent comparison with the A_{1g} features at Γ(1114 cm^{-1}) and X(1108 cm^{-1}). There remains some weak structure, such as that at 926, 1046, and 1149 cm^{-1}, which does not correspond with anything at the critical points considered and probably arises from elsewhere in the Brillouin zone.

Considering the lack of exact energy positions for some of the phonon dispersion curves, the number of assignments which can be made is quite satisfactory, and there is substantial evidence in support of the idea that most of the Raman scatter arises from around the critical points X, L, and W (and perhaps Γ).

CONCLUSION

The polarized second-order Raman spectrum of MgO has been recorded in detail. The data supplement previous investigations of the lattice dynamics of MgO by neutron and infrared measurements. A comparison was made to the two-phonon dispersion curves constructed with the help of these latter measurements. It was concluded that the majority of the strong features in the spectrum arose from scatter in the neighborhood of the critical points Γ, X, L, and W – as generally assumed. The analysis is very promising and would appear to present an ideal opportunity for those working with the lattice dynamics of MgO to test theoretical calculations of the polarizability tensors.

---

†Work supported in part by U.S. Army Research Office, Durham, N.C.

*Present address: Queen Mary College, University of London, London, U.K.

[1]G. Peckham, Proc. Phys. Soc. (London) 90, 657 (1967).

[2]M. J. L. Sangster, G. Peckham, and D. H. Saunderson, J. Phys. C 3, 1026 (1970).

[3]B. Piriou and F. Cabannes, Compt. Rend. 264, 630 (1967). Note that the parity of the TO and TA modes in MgO at L are reversed compared to NaCl. This has given rise to wrong assignments of the infrared-active combinations.

[4]J. R. Jasperse, A. Kahan, J. N. Plendl, and S. S. Mitra, Phys. Rev. 146, 526 (1966).

[5]N. B. Manson (unpublished).

[6]M. J. Sangster and C. W. McCombie, J. Phys. C 3, 1498 (1970).

[7]G. P. Imbush, AEC Report No. M.L.1190, 1964 (unpublished).

[8]M. D. Sturge, Phys. Rev. 140, A880 (1965).

[9]J. P. Mon, J. Phys. 26, 611 (1965); Compt. Rend. 263, 1018 (1966); J. Phys. 28, 886 (1967).

[10]J. P. Mon, Compt. Rend. 266, 1222 (1968).

[11]N. B. Manson, Ph.D. thesis, University of Aberdeen, 1968 (unpublished).

[12]R. Loudon, Advan. Phys. 13, 423 (1964).

[13]H. Poulet, Ann. Phys. (Paris) 10, 908 (1955).

[14]W. G. Nilsen, Phys. Rev. 182, 838 (1969).

[15]T. C. Damen, S. P. S. Porto, and B. Tell, Phys. Rev. 142, 570 (1969).

[16]L. Van Hove, Phys. Rev. 89, 1189 (1953).

[17]F. A. Johnson and R. Loudon, Proc. Roy. Soc. (London) A281, 274 (1964).

[18]E. Burstein, F. A. Johnson, and R. Loudon, Phys. Rev. 139, A1239 (1965).

[19]The dispersion curves are not shown for the critical point W. This is because the 21 branches are too close to be clearly illustrated. The one-phonon dispersion curves at W give two singly degenerate modes of symmetry W_2' or W_1 at 336 and 440 cm^{-1} which are flat in k space. (The assignment of the branches to W_2' or W_1 have not been made. However, this does not affect the Raman-active selection rules.) There are also two doubly degenerate W_3 modes at 403 and 495 cm^{-1}. Away from W the degeneracy is lifted, with the branches having equal but opposite slopes – see Ref. 2.

[20]L. Chen, R. Berenson, and J. L. Birman, Phys. Rev. 170, 639 (1968).